Carbon Balance and Management

RESEARCH

Open Access

Impact of biochar on carbon sequestration in permafrost region of Northeast China

Haiyin Wu[1], Shuying Zang[1,2], Hanxi Wang[1,2*] and Dianfan Guo[1,2]

Abstract

Background Biochar effects on soil organic matter stability in permafrost regions remains poorly understood. To address this knowledge gap, two-cycle incubation experiments using representative forest and peatland soils were conducted from Daxing'anling permafrost region. Soils with corn straw-derived biochar (pyrolyzed at 450 °C, 2 h) were amended at 8% w/w of dry soil weight and systematically measured soil organic carbon (SOC), total nitrogen (TN), dissolved organic carbon (DOC), carbon fractions, microbial community, carbon emission, and CO_2 isotope content.

Results The research indicated that biochar amendment improved physicochemical properties in both soil types. Electrical conductivity increased by 166.62% (forest) and 223.79% (peatland), while SOC increased by 60.57% (forest) and 5.64% (peatland). Mineral-associated organic carbon increased significantly (particularly in forest soils), which also exhibited increases in TN (32.15% at 180 days) and DOC (197.50% at 90 days). Biochar addition reduced the diversity and richness of bacterial communities in forest soils, but had no significant effect on peatlands.

Conclusion Biochar promoted soil aggregate formation, improved soil carbon sequestration capacity, and reduced CO_2 emissions by 19.37% (forest) and 9.70% (peatland). These findings confirmed the dual functionality of biochar in increasing soil carbon storage and reducing carbon emissions. The study provides valuable insights for enhancing carbon management strategies in vulnerable permafrost ecosystems, emphasizing the potential of biochar in soil management.

Keywords Greenhouse gases, Permafrost, Biochar, Carbon fractions, Isotopic tracing

Introduction

The Daxing'anling permafrost region is located at the southern edge of Eurasia high-latitude permafrost belt, which is second-largest permafrost zone of China [1] and characterized by discontinuous permafrost transitioning to continuous formations in northern sectors [2]. Climate warming has elevated temperatures in these permafrost areas, which directly influences active layer thickness dynamics and altered soil moisture-heat transport mechanisms, thereby modifying carbon cycling processes [3]. Soil carbon cycles critically influence both soil quality and greenhouse gas (GHG) emissions [4]. Under combined climate change and human disturbances, the soil organic carbon (SOC) depletion in northeastern the black soil region of China has exceeded 50% [5], which accelerates SOC loss and elevating GHG emissions [6]. Consequently, SOC conservation represents a crucial strategy for climate change mitigation [7] and soil quality enhancement [8].

*Correspondence:
Hanxi Wang
wanghx197@nenu.edu.cn; wanghanxizs1982@126.com
[1]Heilongjiang Province Key Laboratory of Geographical Environment Monitoring and Spatial Information Service in Cold Regions/School of Geographical Sciences, Harbin Normal University, Harbin 150025, China
[2]Heilongjiang Province Collaborative Innovation Center of Cold Region Ecological Safety, Harbin 150025, China

Biochar application enhances SOC sequestration [9] by improving physicochemical and microbial properties [10], stabilizing carbon, reducing GHG emissions [11], and increasing nutrient use efficiency [12]. Long-term SOC increases derive from the inherent stability of biochar and suppression of organic matter mineralization [13, 14]. Interactions between biochar and soil organic matter (SOM) promote organo-mineral complex formation [15] and inhibit SOC mineralization through negative priming effects (PEs) [16]. However, the influence of biochar on carbon emissions remains context-dependent (soil type, biochar feedstock, pyrolysis conditions), and environmental factors [17] may cause increases [18], reductions [19], or neutral effects [20]. Although labile biochar carbon can stimulate microbial co-metabolism and increase emissions transiently [21], long-term mitigation relies on inhibitory mechanisms involving soil property modification, gas adsorption, and microbial activity suppression [22, 23].

Forests and peatlands dominant the Daxing'anling region, which form high-latitude carbon-dense ecosystems [24]. Peatlands exhibit higher SOC density than forests due to temperature- and topography-driven waterlogging that inhibits decomposition [25]. Biochar-induced PEs are regulated by inherent soil properties with SOC content, texture (silt/clay), and pH as key drivers [26–28]. Weaker PEs occur in high-SOC versus low-SOC soils [29], which indicate pre-existing SOC pool size governs responsiveness. Sandy soils exhibit stronger positive PEs than clayey soils due to enhanced microbial accessibility to SOC [27, 30], and biochar-induced pH elevation stimulates microbial activity and intensifies PEs [31]. Identifying such soil-specific mechanisms is essential for developing tailored carbon management strategies.

Converting straw residues into biochar provides a sustainable agricultural waste management strategy [32], which mitigates air pollution and resource waste from open burning. Pyrolysis transforms most organic carbon into recalcitrant aromatic structures, while syngas (e.g., CO, H_2, CH_4) can be utilized for energy to offset carbon emissions [33]. Current permafrost carbon emissions studies primarily focus on three critical seasonal stages (spring thaw period, summer growth season, and autumn freeze period). This research is mainly conducted through short-term experiments examining climate warming [34] and natural freeze-thaw cycles [35] on the GHG fluxes in permafrost regions. However, few studies have systematically monitored carbon emissions across all three periods in permafrost regions. Continuous multi-year (≥ 2 years) data are essential to elucidate long-term carbon emission patterns. To address this gap and evaluate the impact of biochar on carbon dynamics in permafrost, a controlled indoor simulation experiment was conducted encompassing three key seasonal phases.

Clarifying biochar-mediated carbon sequestration requires tracking distinct carbon sources. Soil humus exhibits characteristic carbon isotopic ($\delta^{13}C$) differences between C_3 and C_4 plant origins, while straw-derived biochar possesses a distinct isotopic signature. Carbon isotopes can be used to track carbon sources, the whereabouts of SOC and plant residual carbon under the influence of biochar, and the contribution of biochar to CO_2 emissions [36]. Stable carbon isotope analysis with mixing models were combined to identify different carbon pools in the soil and quantify the impact of biochar on carbon mineralization [37].

Existing biochar research focuses predominantly on agricultural soils, and leaving critical knowledge gaps in permafrost regions are (1) the ability of biochar to enhance SOC stability and reduce carbon emissions, (2) comparative studies on soils with different SOC levels (low-carbon forests versus high-carbon peatlands), and (3) direct evidence (e.g., $\delta^{13}C$-CO_2) for biochar-induced suppression of native SOC mineralization. The objectives address these gaps by (1) characterizing carbon emission dynamics in permafrost soils of forests (low SOC) and peatlands (high SOC) modified with biochar, (2) elucidating the physicochemical and microbial mechanisms that inhibit soil carbon mineralization, and (3) employing $\delta^{13}C$ tracing to differentiate CO_2 sources into natural SOC and biochar. This approach establishes a scientific basis for optimizing biochar-mediated carbon management in permafrost ecosystems.

Materials and methods

Tested soils

The biochar was derived from corn straw, which pyrolyzed at 450 °C for 2 h under a nitrogen (N_2) atmosphere. The properties of biochar can be found in the BC0 experimental group of published literature [38]. Key properties are detailed in Table 1. Topsoil (0–10 cm depth) from the larch (*Larix gmelinii*) forest (122.864 °E, 51.850 °N) and peatland (124.136 °E, 50.424 °N) were collected in the mixed forest-wetland ecosystems of Daxing'anling (Fig. 1a). Sloping terrain supported forests with loamy soil, while low-lying permafrost sustained peat swamps, with a summer water table depth of about 10 cm [39]. Three independent sampling points per site were homogenized from five diagonal subsamples. Samples were transported and stored at 4 °C, then processed through 2-mm sieving to remove stones and roots, followed by moisture content determination. The soils were classified as dark brown Alisols (FAO), with texture of 12.45% sand, 58.89% silt, 28.66% clay for the forest, and 72.95% sand, 27.05% silt for the peatland.

Table 1 Physicochemical properties of corn straw-derived Biochar

	pH		Bulk density (g cm^{-3})		C (wt%)		*N* (wt%)	M_{ad} (wt%)	A_{ad} (wt%)	V_{ad} (wt%)
	8.10 ± 0.16		0.257 ± 0.006		77.30 ± 1.39		0.87 ± 0.13	5.07 ± 0.12	10.11 ± 0.89	7.88 ± 0.55
Biochar	Metallic elements (wt%)					Func-	Particle size	SSA	Pore volume	Permeability
	Mg	K	Ca	Cr	Fe	tional groups	(mm)	(m^2 g^{-1})	(cm^3 g^{-1})	coefficient ($cm{\cdot}s^{-1}$)
	0.84 ± 0.09	1.09 ± 0.12	1.20 ± 0.17	0.37 ± 0.06	0.21 ± 0.05	12	< 2	305.52 ± 9.23	0.098 ± 0.011	0.026 ± 0.008

(1) wt% is the percentage of mass; M_{ad} is sample moisture; V_{ad} stands for volatile matter; A_{ad} is ash content. *ad* is air drying base; SSA is the specific surface area (SSA) of biochar

(2) The functional groups of biochar mainly included -OH, C-H, C = O, -COOH, etc

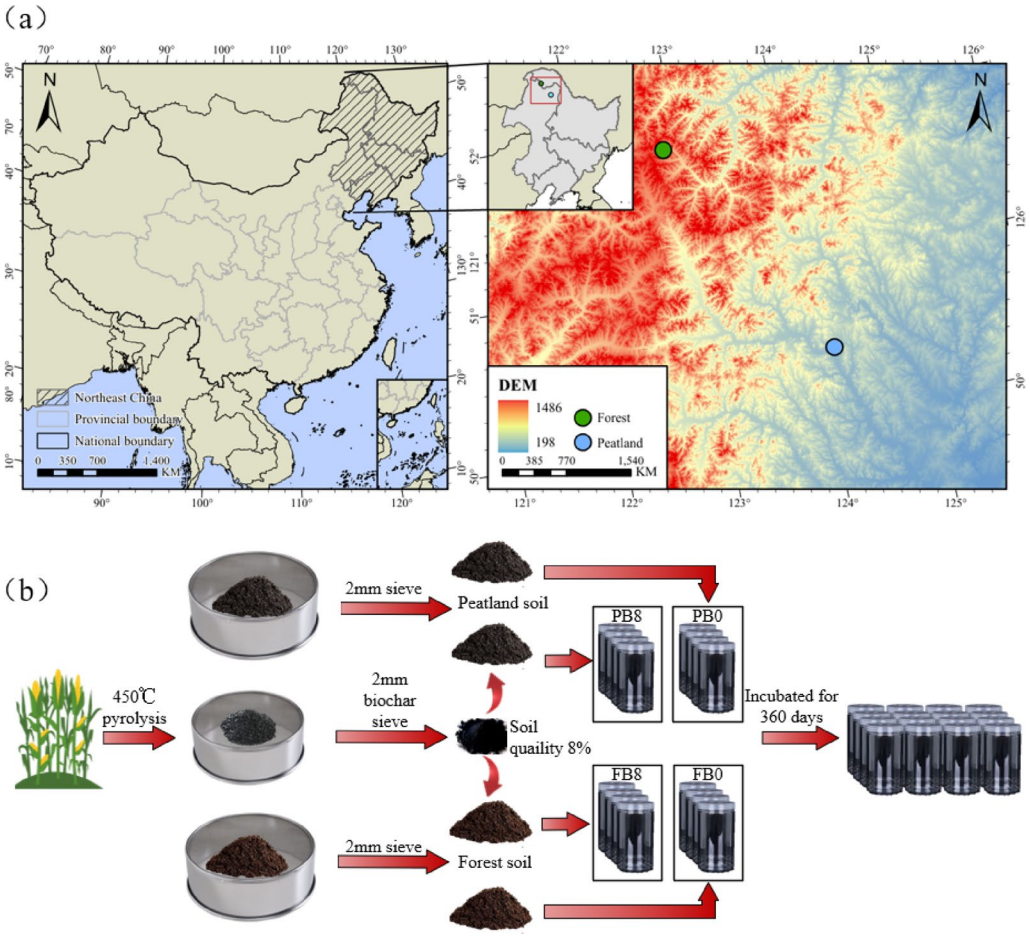

Fig. 1 Location of the research area and experimental flow chart

Experimental description

The optimal amount of biochar is usually less than 10% of the soil dry weight [40, 41]. Therefore, the study established four experimental treatments, each replicated three times: FB0 (forest control), FB8 (forest with 8% biochar, w/w), PB0 (peatland control), and PB8 (peatland with 8% biochar, w/w). Fresh forest soil (957.25 g wet weight; 700 g dry weight) and peatland soil (1391.85 g wet weight; 270 g dry weight) were packed into polymethyl methacrylate (PMMA) columns of uniform volume (Fig. 1b). Soil moisture was maintained at field capacity with ultrapure water additions every three days. Pre-incubation was conducted at 10 ℃ for 15 days under dark conditions to stabilize microbial activity [42].

Incubation occurred in a temperature-controlled, lightproof chamber (Thermo Fisher Scientific, Waltham, MA, USA). Temperature regimes were programmed based on field data recorded at 5 cm soil depth, simulating seasonal phases were spring thaw (0–8 °C), summer growth (10–13-10 °C), and autumn freeze (10–0 °C). Temperatures followed a stepwise progression (0, 1, 3, 5, 6, 8, 10, 12, 13, 11, 11, 10, 10, 7, 7, 3, 1, and 0 °C), with each phase maintained for 10 days. The experiment comprised two consecutive 180-day cycles (total 360 days). Gas was sampled

at 5-day intervals during cycle 1 and 10-day intervals during cycle 2, following system stabilization. Prior to sampling, column lids were opened in a well-ventilated area to equilibrate the headspace. Emissions were quantified by collecting 20 mL headspace samples before and after 5-h containment periods. The carbon isotopic composition of respired CO_2 ($\delta^{13}C_{CO2}$) was analyzed at 60-day intervals (Day 60, 120, 180, 240, 300, and 360).

Analysis methods

Determination of soil physicochemical properties

SSA were determined with an SSA and aperture analyzer (ASAP2460, Micromeritics Instrument Corp, USA). Elemental composition was analyzed using an elemental analyzer (Flash2000, Thermo Fisher Scientific, Italy). Soil physicochemical properties were measured at 90-day intervals (0, 90, 180, 270, 360 days), quantifying total porosity by the ring knife method and electrical conductivity (EC) with a DDBJ-351 L conductivity meter. Soil texture followed USDA classification: sand (> 50 μm), silt (2–50 μm), and clay (< 2 μm). Organic matter removal involved sequential pretreatment with 5% H_2O_2 and 5% HCl, followed by sodium hexametaphosphate dispersion and particle size analysis (Mastersizer 3000, Malvern Panalytical, UK).

Soil permeability was assessed via variable head method with a T55 permeameter (2 m initial head height, ultrapure water interpolation), calculated using Eqs. (1) and (2).

$$k_{\mathrm{T}} = 2.3\frac{aL}{\mathrm{A}t}\lg\frac{H_1}{H_2} \tag{1}$$

$$k_{20} = k_{\mathrm{T}}\frac{\eta_T}{\eta_{20}} \tag{2}$$

where, k_T is the temperature-dependent permeability coefficient, cm s^{-1}; A is the specimen cross-sectional area, cm; a is the variable head pipe cross-sectional area, cm^2; L is the height of the sample, cm; H_1, H_2 is the initial/final water head heights, cm; k_{20} is the permeability coefficient of the sample at standard temperature (20 °C), cm s^{-1}; η_T, η_{20} is the water dynamic viscosity coefficient at T °C and 20 °C, 10^{-6} kPa·s.

Total nitrogen (TN) was quantified by modified Kjeldahl method, while total phosphorus (TP) was quantified by alkali fusion-Mo-Sb anti-spectrophotometry. Soil ammonia nitrogen (NH_4^+-N) and nitrate nitrogen (NO_3^--N) were extracted with 2 M KCl and measured using spectrophotometrically. All analyses were conducted immediately after extraction with a SAN + + continuous-flow analyzer (Skalar Analytical, Netherlands). Soil samples were ground to < 125 μm and analyzed SOC content including the $\delta^{13}C$. Carbonate removal was achieved through 2 M HCl pretreatment, followed by SOC quantification using Multi N/C 2100 analyzer. The $\delta^{13}C$ values was determined using a MAT-253 stable isotope ratio mass spectrometer with zero-blank autosampler. Standard deviations of internal standards were better than ± 0.1‰ for $\delta^{13}C$ values and ± 2% of the value for abundance measurements. Soil dissolved organic carbon (DOC) was analyzed directly by Multi N/C 3100 analyzer, while particulate organic carbon (POC) and mineral-associated organic carbon (MAOC) were separated by 18-h sodium hexametaphosphate dispersion and wet sieving. Then the POC fraction (> 53 μm) and MAOC fraction (< 53 μm) were separated by sieving. Soil of different fractions were dried and ground for organic carbon analysis. Soil pH was measured with a calibrated meter.

Microbiological analysis

Amplicon sequencing of bacterial 16 S rRNA genes (V3-V4 region) and fungal ITS regions were conducted by Majorbio Bio-pharm Technology Co., Ltd (Shanghai, China). Total genomic DNA was extracted from soil samples using the E.Z.N.A.® Soil DNA Kit (Omega Biotek, USA). DNA quality was assessed by 1% agarose gel electrophoresis with concentration and purity measured using a NanoDrop 2000 spectrophotometer (Thermo Scientific, USA). Bacterial V3-V4 regions were amplified with barcoded primers 338 F (5′-ACTCCTACGGG AGGCAGCAG-3′) and 806R (5′-GGACTACHVGGGT-WTCTAAT-3′), while fungal ITS1 regions were amplified with primers ITS1F (5′-CTTGGTCATTTAGAGGA AGTAA-3′) and ITS1R (5′-GCTGCGTTCTTCATCGAT GC-3′). Triplicate PCR reactions per sample minimized technical variation. PCR products were separated on 2% agarose gel electrophoresis, purified using a PCR Clean-Up Kit (YuHua, China), and quantified with a Qubit 4.0 Fluorometer (Thermo Fisher Scientific, USA).

Respiration measurements

Concentrations of CO_2 and CH_4 were quantified using gas chromatography (Agilent 7890B GC System, USA). Calibration occurred every 12th sample using certified GHG standards (National Reference Materials Center, China). Soil GHG emission rates (F, mg·kg^{-1} h^{-1}) were calculated using Eq. (3) [43]. Cumulative soil respiration was calculated using Eq. (4) [44].

$$F = \rho \times \Delta C \times V \times \frac{273}{(273+T)\times W} \tag{3}$$

$$C = \sum\nolimits_{i=1}^{n} \frac{F_i + F_{i+1}}{2} \times (t_{i+1} - t_i) \times 24 \tag{4}$$

where, ρ is the calibration gas concentration, $g{\cdot}L^{-1}$; ΔC is the GHG concentration difference relative to the blank, $mL{\cdot}m^{-3}{\cdot}h^{-1}$; V is the chamber volume, mL; T is the incubation temperature, ℃; W is the soil dry weight, kg. Positive and negative F values indicate net GHG emissions and absorption, respectively.

The $\delta^{13}C_{CO2}$ was analyzed using a CO_2 isotope analyzer (CCIA, ABB, Canada), calibrated with certified reference gas (401.7 ppm CO_2, $\delta^{13}C$ = −20.82‰). Analytical precision (± 0.13‰) was confirmed through repeated measurements. The $\delta^{13}C_{CO2}$ was determined using Eq. (5).

$$\delta^{13}C_{CO2}\ (^{0}/_{00}) = \left(\frac{R_{\text{sample}}}{R_{\text{standard}}} - 1\right) \times 1000 \quad (5)$$

where R_{sample} and R_{sample} represent the $^{13}C/^{12}C$ ratios of samples and Vienna Pee Dee Belemnite (VPDB), respectively.

Biochar-derived carbon contributions were quantified using Eq. 6:

$$f_{biochar} = \frac{\delta^{13}C_{B8} - \delta^{13}C_{B0}}{\delta^{13}C_{\text{biochar}} - \delta^{13}C_{S}} \quad (6)$$

where, $f_{biochar}$ is the biochar-carbon fraction in CO_2; $\delta^{13}C_{B0}$, $\delta^{13}C_{B8}$ is the control and biochar-amended soil isotope signature; $\delta^{13}C_{biochar}$, $\delta^{13}C_S$ is the biochar and native soil isotope signatures.

Statistical analysis

Statistical analysis of microbiome community data was conducted on the Meggie Bioinformatics Cloud Platform. The alpha diversity of the microbiome was calculated using Mothur (version 1.30.2) software, measuring observed species count, Shannon diversity index, and Chao1 richness estimate. Statistical analyses used IBM SPSS Statistics 26. Prior to analysis, data normality was verified using the Shapiro-Wilk test ($p > 0.05$), and homogeneity of variance was confirmed with Levene's test ($p > 0.05$). When data violated these assumptions, appropriate transformations (e.g., logarithmic or square root) were applied to meet ANOVA requirements. Two-way analysis of variance (ANOVA) was performed, followed by Fisher's Least Significant Difference (LSD) post-hoc test to evaluate the effects of biochar application on soil properties. A significance threshold was applied with results deemed statistically significant at $P \leq 0.05$. Effect sizes (η^2) were calculated to quantify the magnitude of significant effects, with $\eta^2 \geq 0.01$, ≥ 0.06, and ≥ 0.14 interpreted as small, medium, and large effects, respectively.

Result

Physicochemical properties

The elemental composition and pore structure characteristics of soil samples are summarized in Table 2. Forest control groups (F0, FB0-M and FB0-E) exhibited a biphasic trend, characterized by an initial increase followed by a decline over the experimental period. Corresponding SSA and pore volume showed parallel temporal patterns. Biochar significantly increased C and N content in forest soils, while other elements remained stable. In peatland controls treatments displayed slight reductions in C, H, and O content, though SSA and pore volume were unaffected. Conversely, biochar-amended peatland soils maintained stable elemental composition throughout incubation period. However, their SSA and pore volume exhibited an initial increase during early phases, followed by a gradual reduction in later stages.

Post-incubation, FB8 exhibited EC increases of 166.62% relative to FB0, while PB8 showed increases of 223.79% compared to PB0 (Table 3). Compared to FB0, the permeability of FB8 reduced by 73.10% in cycle 1 and 73.76% in cycle 2. In contrast, peatland soil exhibited only transient permeability reductions, with a 57.00% decrease during the initial 180 days, but no sustained long-term

Table 2 Element content and pore structure in different experimental groups

Experimental group	Element content				Pore structure	
	C (wt%)	O (wt%)	*N* (wt%)	H (wt%)	BET ($m^2 \cdot g^{-1}$)	Micropore volume ($cm^3 \cdot g^{-1}$)
F0	4.43 ± 0.07	12.93 ± 0.07	0.19 ± 0.03	1.63 ± 0.06	153.07 ± 10.26	0.065 ± 0.009
FB0-M	4.72 ± 0.02	13.02 ± 0.08	0.19 ± 0.03	1.71 ± 0.13	160.42 ± 11.17	0.082 ± 0.015
FB0-E	4.53 ± 0.06	12.36 ± 0.53	0.18 ± 0.03	1.57 ± 0.07	66.56 ± 0.08	0.026 ± 0.004
FB8-M	7.67 ± 0.22	12.76 ± 0.45	0.26 ± 0.01	1.62 ± 0.05	274.97 ± 25.61	0.133 ± 0.023
FB8-E	7.84 ± 0.08	12.68 ± 0.41	0.25 ± 0.01	1.60 ± 0.02	257.31 ± 23.51	0.121 ± 0.019
P0	40.74 ± 0.24	35.60 ± 0.25	2.06 ± 0.04	5.18 ± 0.16	165.22 ± 28.16	0.071 ± 0.011
PB0-M	40.56 ± 0.18	35.00 ± 0.50	1.93 ± 0.05	5.13 ± 0.21	152.29 ± 12.39	0.064 ± 0.017
PB0-E	38.93 ± 0.44	34.36 ± 0.41	2.13 ± 0.07	5.07 ± 0.29	162.19 ± 13.07	0.066 ± 0.023
PB8-M	40.17 ± 0.28	33.58 ± 1.18	2.11 ± 0.07	4.87 ± 0.19	570.02 ± 35.21	0.346 ± 0.052
PB8-E	41.96 ± 0.26	32.31 ± 0.50	2.00 ± 0.04	4.94 ± 0.05	272.68 ± 19.35	0.123 ± 0.029

(1) F0 and P0 represent initial forest and peatland soil states, respectively; (2) FB0-M, FB8-M, PB0-M, and PB8-M represent soil mid-cycle elemental content; (3) FB0-E, FB8-E, PB0-E and PB8-E represent soil end-cycle elemental content

Table 3 Permeability coefficient and EC in different experimental groups

Experimental group	EC ($\mu s\ cm^{-1}$)	Permeability coefficient ($cm\ s^{-1}$)	Experimental group	EC ($\mu s\ cm^{-1}$)	Permeability coefficient ($cm\ s^{-1}$)
F0	24.78 ± 5.47	0.000403 ± 0.000021	P0	126.70 ± 10.59	0.000257 ± 0.000017
FB0-1	39.9 ± 8.52a	0.000394 ± 0.000040a	PB0-1	46.27 ± 5.67a	0.000493 ± 0.000052a
FB8-1	122.77 ± 13.74b	0.000106 ± 0.000024b	PB8-1	112.07 ± 5.45b	0.000212 ± 0.000068b
FB0-2	36.37 ± 7.64a	0.000282 ± 0.000005a	PB0-2	59.47 ± 5.33a	0.000273 ± 0.000106a
FB8-2	96.97 ± 8.33b	0.000074 ± 0.000001b	PB8-2	192.63 ± 9.25b	0.000212 ± 0.000053a

F0 and P0 represent initial forest and peatland soil; FB0-1, FB8-1, PB0-1, and PB8-1 represent soil EC and permeability coefficient of cycle 1; FB0-2, FB8-2, PB0-2 and PB8-2 represent soil EC and permeability coefficient of cycle 2. Lowercase letters denote significant differences ($P < 0.05$) between biochar-amended and control soils

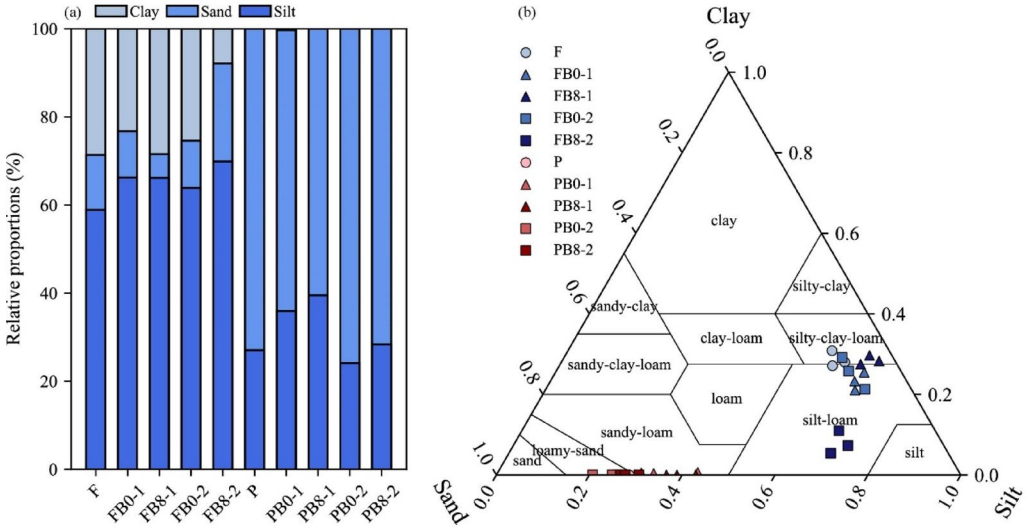

Fig. 2 Changes in soil particle size distribution: **a**. Relative proportion changes across treatment groups post-incubation (cycles 1 and 2), **b**. USDA textural classification via ternary diagram of treatment groups post-incubation (cycles 1 and 2)

effects (Table 3). USDA texture analysis classified forests as silty loam and silty clay, whereas peatland soils were dominated by loam and sandy loam (Fig. 2b). Biochar induces changes in soil particle size distribution: in forest soils, sand content increased by 92.83%, while clay content decreased by 68.92%. In peatland soil, biochar addition increased sand content by 5.63% (Fig. 2a).

Relative to FB0, pH decreases of 4.60% (cycle 1) and 5.59% (cycle 2) were observed in FB8. In contrast, peatland soils-maintained pH stability regardless of biochar application. Compared to FB0, FB8 exhibited TP increases of 26.80 and 34.84% in cycle 1, while PB8 showed greater increases of 38.85 and 53.36% relative to FB0 (Fig. 3e). However, heterogeneous variance in cycle 2 rendered TP changes statistically insignificant. At 90, 180, 270, and 360 days, the TN content in FB8 increased by 16.4%, 32.15%, 27.25%, and 7.23%, respectively, compared to FB0 (Fig. 3f). The C/N ratio of FB8 increased by 101.52%, 110.45%, 38.58%, and 50.28% at 90, 180, 270, and 360 days, respectively, compared to FB0. In contrast, PB8 showed increases of 7.09%, 10.29%, 12.34%, and 1.45% at the corresponding time points relative to PB0. Furthermore, the addition of biochar significantly affects the soil C/N ratio (Table 4).

The SOC in FB8 increased by 135.94%, 177.97%, 82.18%, and 60.57% at 90, 180, 270, and 360 days, respectively, compared to FB0 ($p < 0.05$). In contrast, PB8 exhibited smaller SOC increases of 0.64%, 10.22%, 4.42%, and 5.64% at the same intervals relative to PB0 (Fig. 3a). The DOC content was significantly affected by incubation time in both ecosystems (Table 4, $p < 0.05$). Specifically, DOC in FB8 increased by 197.50%, 30.62%, 23.73%, and 0.62% at 90, 180, 270, and 360 days, respectively, relative to FB0 (Fig. 3b). The impact of biochar on DOC in forest attenuated temporally, exhibiting a progressive reduction toward the end of incubation.

Biochar application exhibited a significant positive correlation with MAOC in all tested soils (Table 4). FB8 showed increases of 103.37% in cycle 1 and 175.89% in cycle 2 relative to FB0. Peatland MAOC (PB8) displayed smaller but consistent increases of 41.76% (cycle 1) and 3.05% (cycle 2) compared to PB0. Conversely, the impact of biochar on POC diverged markedly between ecosystems: forest soils demonstrated significant positive correlations with POC content, whereas peatland soils

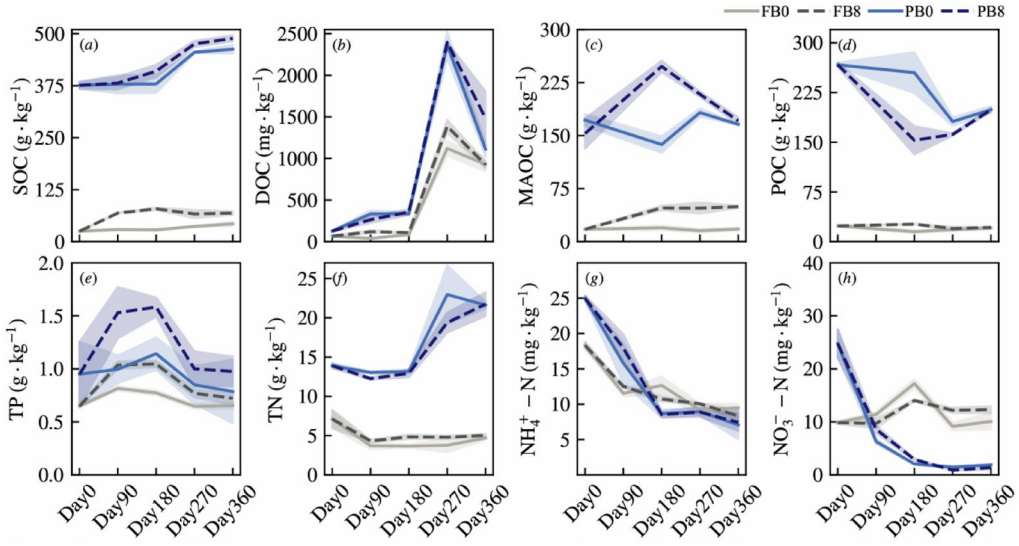

Fig. 3 Soil chemical properties of SOC (a), DOC (b), MAOC (c), POC (d), TP (e), TN (f), NH_4^+-N (g) and NO_3^--N (h) accumulated changes from forests and peatland under biochar addition for 360 days incubation

Table 4 Two-way ANOVA results of soil properties after biochar addition after two incubation cycles

Soil types	Experimental conditions	SOC		DOC		POC	
		P	η^2	P	η^2	P	η^2
Forest	Biochar	0.000*	0.881	0.827	/	0.000*	0.569
	Incubation time	0.377	/	0.000*	0.991	0.803	/
	Biochar × incubation time	0.001*	0.091	0.000*	0.008	0.001*	0.407
Peatland	Biochar	0.020*	0.104	0.000*	0.074	0.000*	0.577
	Incubation time	0.000*	0.847	0.000*	0.953	0.024*	0.024
	Biochar × incubation time	0.813	/	0.000*	0.064	0.000*	0.575
Soil types	Experimental conditions	MAOC		TN		C/N	
		P	η^2	P	η^2	P	η^2
Forest	Biochar	0.000*	0.945	0.000*	0.453	0.000*	0.868
	Incubation time	0.968	/	0.002*	0.294	0.221	/
	Biochar × incubation time	0.31	/	0.013*	0.14	0.004*	0.081
Peatland	Biochar	0.000*	0.607	0.887	/	0.077*	0.031
	Incubation time	0.001*	0.057	0.000*	0.975	0.000*	0.867
	Biochar × incubation time	0.000*	0.514	0.72	/	0.137	/

The "*" indicated significant effect ($P < 0.05$)

exhibited negative trends (Table 4; Fig. 3d). Specifically, POC content in FB8 (cycle 1) and FB8 (cycle 2) increased by 50.33% and 4.59% respectively, relative to FB0. In contrast, PB8 (cycle 1) and PB8 (cycle 2) decreased by 40.03% and 0.05%, respectively, compared to PB0.

Microbial abundance and diversity

Microbial communities were consolidated by merging OTUs with relative abundances below 0.05% into "Others", which yielded eight bacterial and five fungal phyla (Fig. 4a). In forest soils, *Pseudomonadota*, *Acidobacteriota*, *Actinomycetota*, *Chloroflexota*, and *Gemmatimonadota* dominated the bacterial community, collectively comprising > 75% of total sequences, which reflected typical aerobic and litter-input ecosystems. Peatland soils exhibited significant enrichment of *Verrucomicrobiota* and *Bacteroidota*, which functionally replaced *Gemmatimonadota*, indicating anaerobic, organic-rich conditions promoted methanotrophs (*Verrucomicrobiota*) and fermenters (*Bacteroidota*). Fungal communities in both habitats were dominated by *Ascomycota* and *Mortierellomycota*. Biochar amendment significantly increased the abundances of *Pseudomonadota*, *Actinomycetota*, *Chloroflexota*, *Gemmatimonadota*, and *Ascomycota* abundances in forest soils while reducing *Acidobacteriota*, *Verrucomicrobiota*, and *Mortierellomycota*. In contrast, peatland soils showed no significant alterations except decreased *Ascomycota* and increased *Mortierellomycota* abundances.

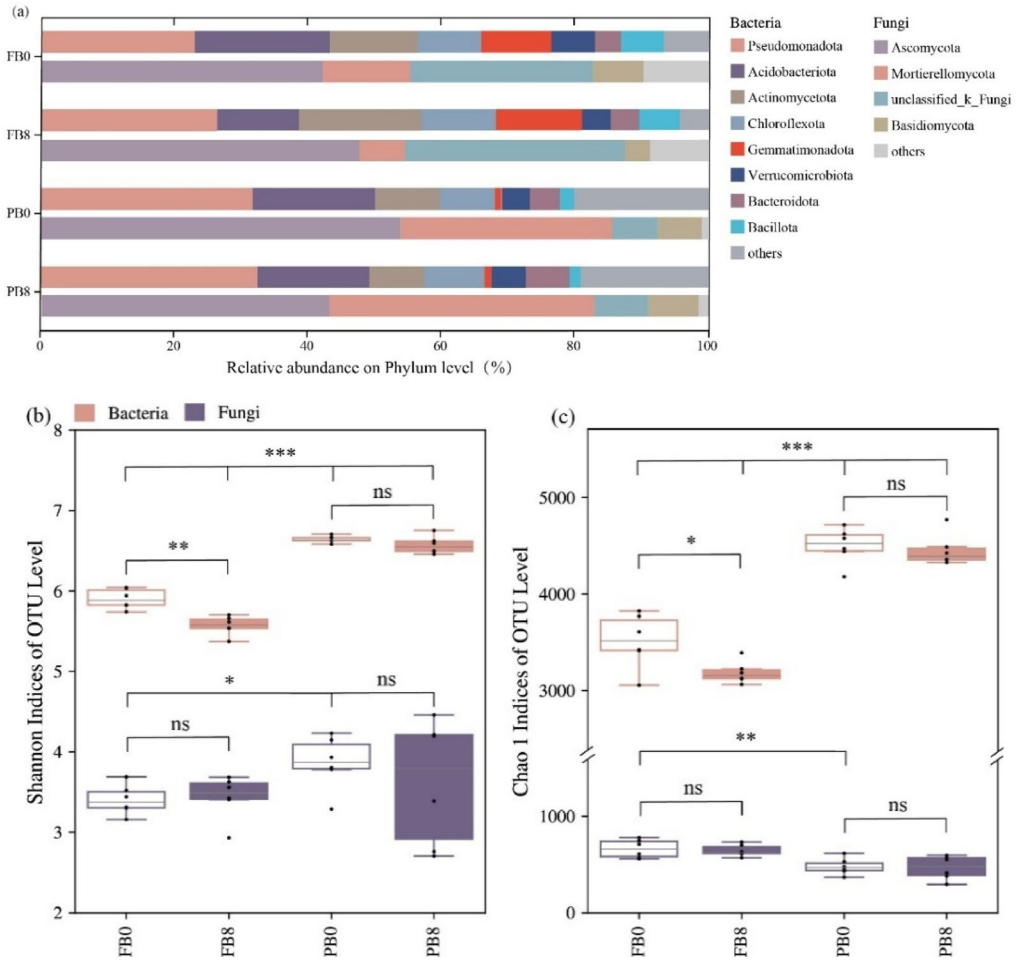

Fig. 4 The relative abundance and community diversity of soil bacteria and fungi in the different treatment groups of forests and peatlands at the end of the cultivation period (**(a)** Changes in the relative abundance of bacteria and fungi at different treatment levels. **(b)** and **(c)** represent the changes in the diversity indices of soil bacterial and fungal communities (Shannon and Chao 1) for each treatment group, respectively. * Indicates significant differences at the 0.05 level, ** indicates significant differences at the 0.01 level, and *** indicates significant differences at the 0.001 level.)

Bacterial and fungal community diversity responded differentially to biochar amendment in forest versus peatland soils (Fig. 4b and c). Peatlands exhibited significantly higher bacterial Shannon diversity and Chao1 richness than forests ($P<0.05$). Although fungal Shannon index was higher in peatlands, their fungal Chao1 index was significantly lower than in forests. In biochar-amended forest soils (FB8 vs. FB0), bacterial Shannon and Chao1 indices declined by 6.57% and 11.73% ($P<0.05$), respectively, with no significant changes in fungal diversity.

Soil carbon emission

CO_2 emission rates and cumulative emissions in biochar-amended soils exhibited pronounced seasonal variability (Fig. 5). In FB8, cumulative CO_2 emissions decreased by 33.61% (Spring 1), 13.80% (Summer 1), and 29.64% (Autumn 1) during cycle 1, and by 65.53% (Spring 2), 14.64% (Summer 2), and 19.37% (Autumn 2) during cycle 2, relative to FB0. The mitigation efficacy of biochar was most pronounced during the spring thaw period, followed by the autumn freeze and summer growth periods. In PB8, cumulative CO_2 emissions showed smaller, non-significant reductions: 13.82% (Spring 1), 8.05% (Summer 1), and 4.95% (Autumn 1) in cycle 1, and 8.86% (Spring 2), 12.33% (Summer 2), and 9.70% (Autumn 2) in cycle 2 compared to PB0.

In FB8, CH_4 uptake decreased by 64.62% (Spring1), 48.28% (Summer1), and 32.30% (Autumn1) during cycle 1, and by 44.07% (Spring2), 26.84% (Summer2), and 46.94% (Autumn2) during cycle 2 compared to FB0 (Fig. 5). The most significant reduction occurred during the spring thaw period of cycle 1. In PB8, CH_4 emissions decreased by 29.59% (Spring1), 22.19% (Summer1), and 52.70% (Autumn1) in cycle 1, and by 34.57% (Spring2), 33.62% (Summer2), and 28.07% (Autumn2) in cycle 2 relative to PB0. The inhibitory effect of biochar on CH_4 uptake peaked during spring thaw in forest soils, whereas the strongest suppression in peatland soils occurred

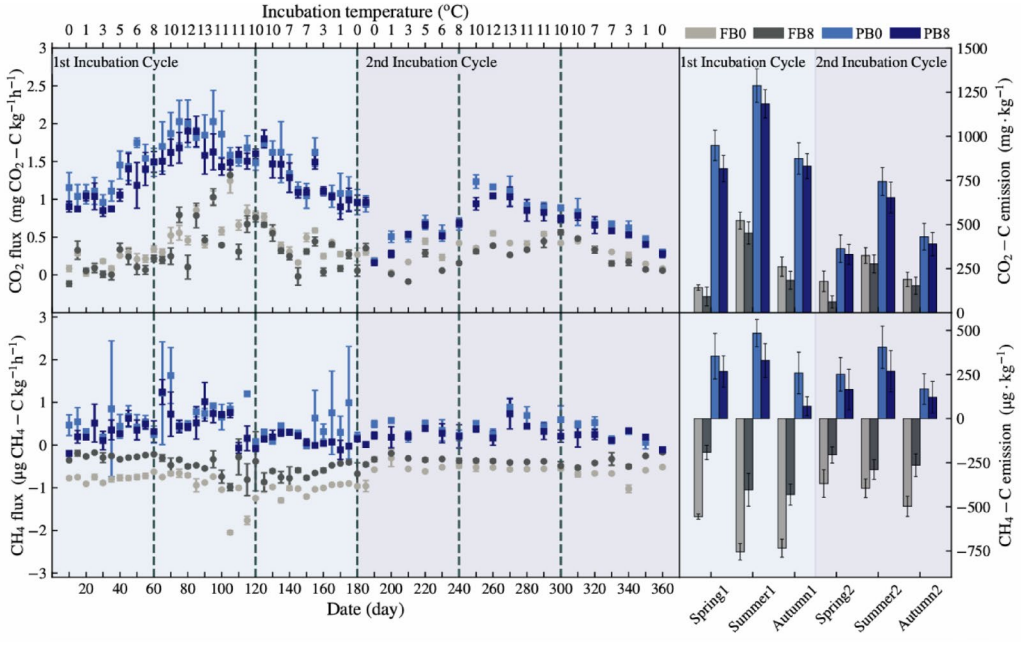

Fig. 5 CO_2 and CH_4 emission dynamics in forest and peatland soils under biochar addition across two incubation cycles (Error bars indicate standard error (SE), and color-coded shading distinguishes between cycles.)

Table 5 The $\delta^{13}C_{CO2}$ values of soil CO_2 emissions under different treatment groups with the addition of biochar, as well as the CO_2 emission, soil-derived CO_2 emissions, and biochar-derived CO_2 emissions during the incubation experiment

Soil types	Time (day)	$\delta^{13}C_{CO2\text{-}B0}$ (‰)	$\delta^{13}C_{CO2\text{-}B8}$ (‰)	CO_2 emission rate (mg CO_2-C $kg^{-1}h^{-1}$)	Soil - CO_2 emission rate (mg CO_2-C $kg^{-1}h^{-1}$)	Biochar - CO_2 emission rate (mg CO_2-C $kg^{-1}h^{-1}$)	$f_{biochar}$
Forest	60	−8.424	−7.513	0.1957	0.1702	0.0254	0.130
	120	−3.072	−0.236	0.6628	0.3937	0.2691	0.406
	180	−4.225	−3.641	0.3536	0.3239	0.0297	0.084
	240	−7.098	−6.632	0.1574	0.1469	0.0105	0.067
	300	−10.191	−9.376	0.5641	0.4981	0.0660	0.117
	360	−10.659	−10.056	0.0580	0.0530	0.0050	0.086
Wetland	60	−8.055	−7.868	1.5038	1.4752	0.0286	0.019
	120	−6.850	-5.116	1.7991	1.4789	0.3202	0.178
	180	−5.796	−4.902	0.9611	0.8726	0.0884	0.092
	240	−6.749	−5.878	0.6811	0.6205	0.0606	0.089
	300	−9.732	−8.672	0.4934	0.4396	0.0538	0.109
	360	−10.165	−9.469	0.2817	0.2617	0.0200	0.071

$\delta^{13}C_{CO2\text{-}B0}$ and $\delta^{13}C_{CO2\text{-}B8}$ represent the soil CO_2 isotope measurement values for the control group and the biochar treatment group, respectively

during autumn freeze (cycle 1). Stabilized inhibition effects were maintained across both ecosystems in cycle 2, which suggested sustained biochar efficacy.

Carbon isotopes

GHG emissions analysis revealed variable decomposition rates in active SOC pools over the 12-month incubation. Temporal $\delta^{13}C_{CO2}$ shifts reflected evolving carbon source contributions (Table 5). Initial $\delta^{13}C_{CO2}$ enrichment was observed, peaking at −3.072 (FB0) and − 0.236 (FB8) by day 120 in forest soils, and − 5.796 (PB0) and − 4.902 (PB8) by day 180 in peatlands. Subsequent depletion occurred, which reached minimum values of −10.659 (FB0), −10.056 (FB8), −10.165 (PB0), and − 9.469 (PB8) by day 360. The contribution of biochar-derived carbon followed a consistent trend across the entire ecosystem (an initial increase peaking at day 120). Among these, the total CO_2 emission rate for forest FB8 was 0.6628 mg $kg^{-1}h^{-1}$ with 40.6% derived from biochar, amounting to 0.2691 mg $kg^{-1}h^{-1}$. The CO_2 emission rate from soil SOC was 0.3937 mg $kg^{-1}h^{-1}$. For peat PB8, the total CO_2 emission rate was 1.7991 mg $kg^{-1}h^{-1}$ with 17.8% coming from biochar, which was 0.3202 mg $kg^{-1}h^{-1}$. While the CO_2

emission rate from soil SOC stood at 1.4789 mg $kg^{-1}h^{-1}$. Following this, a decline stabilized around 10%.

For FB8, the cumulative CO_2 emission reached 1218.540 mg kg^{-1} at the end of incubation (Table 5), of which 260.536 mg kg^{-1} originated from biochar-derived carbon. Given a soil dry weight of 0.7 kg, this translates to an absolute biochar-CO_2 emission of 182.375 mg. Based on the biochar carbon content (77.3 wt%, Table 1), the mineralized biochar-C during the 360-day incubation was calculated as 0.064 g. With 56 g of biochar-C initially applied in FB8, the annual mineralization rate was extrapolated to 0.065 g $year^{-1}$. Consequently, the theoretical persistence of biochar in forest soil was estimated at approximately 875 years. Similarly, for PB8, biochar-C consumption was 0.041 g over 360 days, against an initial application of 21.6 g biochar-C. This yielded an extrapolated annual mineralization rate of 0.042 g $year^{-1}$ and a projected biochar persistence of 527 years.

Discussion

Responses of soil properties to Biochar addition

Biochar significantly increased EC in both soils, possibly due to their inherent high EC and water-soluble cation content. The increased concentration of soluble salts reduces soil colloid dispersion and promotes flocculation [45], a process that is hypothesized to enhance the aggregation mechanism in this unstable state, thereby improving the stability of soil aggregates [46, 47]. Soil permeability, a critical indicator of plant root respiration and soil quality, was significantly reduced by biochar application (Table 3). The applied biochar exhibited a highly porous structure, with a mean pore volume of 0.098 ± 0.011 $cm^3 g^{-1}$, porosity of 60.94 ± 6.62%, and SSA of 305.52 ± 9.23 $m^2 g^{-1}$ (Table 1). Biochar did not function act as a soil skeleton with particle sizes (< 2 mm). However, its high SSA facilitated clay particle absorption [48], thereby reducing soil pore space. Biochar addition altered soil particle size distribution, with pronounced effects in forest soils but minimal impacts in peatlands.

Nitrogen and phosphorus contents are critical to soil nutrient cycling and SOC stabilization. Biochar increased the TP content in both soils during early incubation stages but had no significant effect in the later stages (Fig. 3e). The observed increase in soil TP following biochar addition has been widely documented [49, 50]. Biochar also significantly increased the TN content of forest soils (Fig. 3f). The soil C: N ratio increased with biochar addition, attributable to its inherently high carbon content.

Responses of soil carbon fractions to Biochar addition

Biochar amendment increased SOC content. Biochar pyrolyzed at 400 and 600 ℃ was shown to convert over 82% of labile carbon into aromatic structures [51]. It enhanced soil cation exchange capacity, water retention, and organic matter content, which promoted soil aggregate formation [52]. These aggregates function as primary SOC reservoirs by physically isolating and encapsulating organic carbon, thereby inhibiting microbial decomposition [53]. Furthermore, microaggregate organo-mineral complexes enhance long-term carbon stabilization [54]. Soil DOC content is influenced by SOC and moisture. Labile carbon derived from biochar contributes to higher DOC levels [55], which are readily utilized by microorganisms [56]. However, prolonged incubation reduces this effect as biochar-derived DOC decomposes and adsorption capacity equilibrates [57]. DOC concentration is positively correlated with soil moisture [58], which accounts for elevated DOC levels in peatlands due to their higher moisture content. However, excessive moisture in peatlands limits the ability of biochar to regulate DOC dynamics [59].

Biochar modified soil carbon fractions, MAOC and POC increased in forest soils, whereas peatlands showed MAOC enhancement with POC reduction (Fig. 3c and d). This divergence reflects ecosystem-specific mechanisms. In low-SOC forests, biochar was classified as POC or a substance with similar particle size [60] and promoted aggregate formation [61], which physically protected native POC while reducing decomposition [62]. Meanwhile, the long-term regulatory effect of biochar on soil carbon components may be closely related to its chemical aging process. Subsequent soil oxidation increased biochar's carboxyl (-COOH) and carbonyl (C = O) groups [63], which enhances mineral complexation, facilitated the formation of organic-mineral complexes [64, 65], and transformed POC into MAOC. This explained greater MAOC increase in Cycle 2 compared to Cycle 1 in forest soils. Conversely, in anaerobic peatlands, the porous structure of biochar enhanced local aeration [66], which accelerated aerobic decomposition of protected POC (e.g., partially decomposed fibers/lignin) [67]. Concurrently, aging-induced pore collapse [68, 69] reduced SSA in PB8 from 570.02 to 272.68 $m^2 g^{-1}$ (Table 2), which weakened physical unstable carbon protection (Fig. 3d). Future studies should quantify aging rates by tracking functional group evolution during freeze-thaw cycles, which fragment particles and expose fresh oxidative surfaces.

While biochar universally enhances carbon stabilization, its net effect depends on ecosystem properties. For low-SOC forests, the addition of biochar shows significant potential to simultaneously increase both labile (POC) and stable (MAOC) carbon pools, which made it an efficient carbon sequestration and emission reduction strategy. However, it risks accelerating labile carbon decomposition in high-SOC peatlands, which causes transient carbon loss. When biochar was applied in such ecosystems, the potential risks of carbon loss against the

long-term net carbon sequestration benefits were thoroughly evaluated.

Carbon emissions as influenced by Biochar application

Biochar induced sustained reduction in forest soil CO_2 emissions over 360 days, significantly reducing cumulative emissions (Fig. 5). This aligns with mitigation effects in silt loam forests [70], with quantified potential reaching up to 0.92 Gt CO_2 yr^{-1} [71]. The macropore structure and adsorption capacity of biochar stabilize SOC through pore occlusion and organo-mineral binding. This reduces the CO_2 mineralization rate by inhibiting and altering microbial activity [72]. Increased soil C: N ratios following biochar amendment (Table 4) were correlated with reduced decomposition rates [73], further suppressing mineralization. A negative correlation between biochar C: N ratios and cumulative CO_2-C emissions was confirmed [74]. Reduced soil permeability (Table 3) and restricted gas diffusion due to biochar-induced water retention alterations were identified as contributing mechanisms. Enhanced microbial carbon use efficiency following biochar addition was shown to decrease primary SOC mineralization [75].

A study based on Florida temperate soils found that biochar produced from herbaceous materials at low pyrolysis temperatures (such as 250 °C and 400 °C) typically promotes CO_2 emissions particularly during the early stages of incubation, which attributed to the unstable components of biochar and the co-metabolism of microorganisms [21]. However, the study significantly inhibited CO_2 emissions at all seasonal stages, even in the early stages of incubation (Fig. 5). The difference is mainly attributed to key variations in experimental conditions and environmental contexts, the soil in this study has a high SOC content (Fig. 3), where organic-mineral complexes formed in high SOC environments may simultaneously stabilize both the existing SOC and the newly added biochar carbon [15], thereby masking potential positive stimulation effects in the early stages of incubation. Furthermore, the low incubation temperatures (0–10 °C) during early period suppressed microbial activity, which inhibited the likelihood of increased CO_2 emissions in the early stage.

$\delta^{13}C$ analysis quantified the contribution of biochar to soil GHG emissions. Lignin and lipids in soil were ^{13}C depleted, while sugars, amino acids and hemicellulose were ^{13}C enriched [76, 77]. Glucose and sucrose, which are ^{13}C rich substrates, were preferentially degraded [78, 79]. Their increasing contribution to CO_2 emissions during the early incubation period resulted in a gradual rise in $\delta^{13}C_{CO2}$ values. $\delta^{13}C_{CO2}$ reached its peak at 120 days in forest soil, but this peak was delayed until 180 days in peatland due to the high porosity and water retention capacity of soil that extended oxygen diffusion pathways. These peaks represented the maximum contribution of ^{13}C enriched substrates to CO_2 production. As these readily degradable substrates became depleted, microbial communities increasingly decomposed ^{13}C depleted organic matter, which led to a subsequent decrease in $\delta^{13}C_{CO2}$ values. In biochar-amended soils, the instability of organic carbon components in biochar led to its mineralization during the early stages of incubation [80], which resulted in a peak of $\delta^{13}C_{CO2}$ in forest and peatland soils at 120 days. Among this, $f_{biochar}$ in forest soil accounted for 0.406, supporting the assertion. This stabilized near 10% after depletion of unstable fractions, which confirmed minimal emissions from stable carbon.

Biochar enriches *Actinobacteria* with complex organic matter degradation capabilities in forest soils [81, 82], and this was possibly through specialized niches provided by the biochar itself or the adsorbed complex carbon sources. The competitive advantage of *Actinobacteria* suppresses other bacterial groups through resource competition (carbon/nitrogen/space) and antibiotic secretion [81], which leads to a decrease in bacterial diversity (Fig. 2b and c). Although the reduction in diversity indicates functional simplification, *Actinobacteria* effectively utilize carbon derived from biochar and recalcitrant organic matter, which reduces the mineralization demands of native SOM [83]. This altered metabolic strategy interacts synergistically with the improved soil properties conferred by biochar, which enhanced carbon retention and establishing *Actinobacteria* as core biotic factors in carbon mitigation in forest soils. Cross-domain interactions further regulate microbial balance, decomposition intermediates derived from *Actinobacteria* may provide substrates for fungi such as *Mortierellomycota* [84], while the reduction in bacterial diversity alleviates competition pressure between bacteria and fungi.

Biochar reduced the cumulative oxidation of CH_4 in forest soils throughout the incubation period (Fig. 5). Soil TN content was increased by biochar amendment (Table 4; Fig. 3f). The presence of metal ions and organic matter in biochar (Table 1) was found to inhibit CH_4 oxidation through interactions with methanotrophic bacteria. The CH_4 oxidation rate was reduced or maintained at baseline levels due to inhibitory compounds in biochar, which included organic matter and metals [85]. Soil moisture alterations were shown to affect the exchange of CH_4 and O_2 between soil and the atmosphere [86], modify oxidation-reduction potentials [87], and regulated methanogen and methanotrophic bacterial activity that governs CH_4 oxidation. Biochar application was associated with reduced soil permeability (Table 3) and enhanced the water retention capacity.

Biochar reduced the cumulative emissions of CH_4 from peatland soils (Fig. 5). Soil NO_3^--N content was found to increase (Fig. 3h), which correlated with reduced CH_4

production. High soil moisture restricted CH_4 and O_2 diffusion, thereby limiting CH_4 depletion rates. Biochar-induced pore space expansion was counteracted by water saturation, which resulted in minimal aeration improvements. Elevated moisture levels suppressed microbial activity through restricted O_2 diffusion, delaying organic matter decomposition derived from biochar and extending CH_4 oxidation duration. In waterlogged conditions, CH_4 emissions were further reduced through methanogen inhibition, methanotroph stimulation, and enhanced CH_4 adsorption [88].

Limitations and prospects

This study systematically evaluated biochar-induced changes in permafrost soil properties and carbon mitigation mechanisms under simulated seasonal conditions, yet experimental limitations persist. Despite efforts to approximate field conditions, the indoor incubation system cannot fully replicate complex natural ecosystems due to the absence of live root systems with associated rhizosphere processes (carbon inputs, microbial interactions). The inability to reproduce physical freeze-thaw disturbances (e.g., soil structure disruption and protected organic matter release) despite temperature simulation, and the exclusion of natural variables including precipitation dynamics, wind-driven gas exchange, faunal activity, and soil-permafrost spatial heterogeneity. Future research should therefore integrate controlled experiments with long-term field monitoring to (1) quantify multi-year GHG fluxes, (2) assess biochar-vegetation interactions, and (3) evaluate freeze-thaw impacts on biochar stability.

Additionally, optimizing and modifying biochar research holds promise for further enhancing its efficacy in reducing soil carbon emissions, and future studies should strengthen experimental exploration targeting modified biochar. Future field studies should pay special attention to the influence of particle size on the mobility and spatial distribution of biochar. For field application, high-pressure injection of granular material into permafrost soils has been proposed as a technique for large-scale soil amendment [89]. However, complex terrain (slopes, obstacles) impedes equipment transport and risks root damage. Biochar application is better suited to specific scenarios such as ecological restoration (e.g., post-fire, post-logging, eroded areas), contaminated soil remediation, or soil improvement in production-oriented plantations.

Conclusions and recommendations

A 360-day incubation study in permafrost forest and peatland soils showed that biochar application increased SOC content, reduced permeability, and enhanced silt fraction stabilization. Biochar effectively reduced soil CO_2 emissions, forest soil CH_4 uptake, and peatland soil CH_4 emissions. *Actinobacteria* enrichment and the resulting decline in bacterial diversity constitute the central biological driver of carbon mitigation in forest soils. For soil gas isotope analysis, the early contribution of biochar to soil GHG emissions was related to the unstable C in biochar, which was preferentially mineralized to a certain extent compared with primary SOC. But this tends to stabilize after 120 days of incubation. This confirms the potential of biochar to reduce soil carbon emissions and enhance carbon storage in permafrost areas. The study highlights the potential of biochar to mitigate permafrost carbon-climate feedback by strategically modulating soil physicochemical properties (e.g., C: N ratio, aggregate formation). These findings advocate for optimized biochar deployment as a key strategy for regulating carbon emissions in vulnerable permafrost ecosystems.

Acknowledgements
We appreciate the efforts made by the editors and reviewers on this paper. We appreciate the efforts made by the reviewers and editors on this paper.

Author contributions
Haiyin Wu: Data curation, Formal analysis, Investigation, Methodology, Resources, Software, Supervision, Visualization, Writing – original draft. Shuying Zang: Funding acquisition, Methodology, Resources, Validation, Writing – review & editing. Hanxi Wang: Conceptualization, Methodology, Funding acquisition, Software, Project administration, Supervision, Writing – review & editing. Dianfan Guo: Formal analysis, Investigation, Software, Validation, Writing – original draft. All authors approved the final manuscript as submitted and agree to be accountable for all aspects of the work.

Funding
The present study was gratefully supported by the Science & Technology Fundamental Resources Investigation Program (No. 2022FY100701) and High-level Talent Foundation Project of Harbin Normal University (No. 1305124219).

Data availability
No datasets were generated or analysed during the current study.

Declarations

Ethics approval and consent to participate
Not applicable.

Consent for publication
Not applicable.

Competing interests
The authors declare no competing interests.

Received: 21 May 2025 / Accepted: 2 October 2025
Published online: 25 October 2025

References

1. Qiu L, Shan W, Guo Y, Zhang C, Liu S, Yan A. Spatiotemporal dynamics of vegetation response to permafrost degradation in Northeast China. J Arid Land. 2024;16(11):1562–83.
2. Han Y, Li X, Cai H, Liu J, Chen K. Effects of forest fires on soil carbon and nitrogen storages in thepermafrost region in the Da xing'anling Mountains, NE China. J Glaciol Geocryol. 2024;46(6):1883–95.

3. Chang Z, Qi P, Zhang G, Sun Y, Tang X, Jiang M, Sun J, Li Z. Latitudinal characteristics of frozen soil degradation and their response to climate change in a high-latitude water tower. CATENA. 2022;214:106272.
4. Song Y, Zou Y, Wang G, Yu X. Altered soil carbon and nitrogen cycles due to the freeze-thaw effect: a meta-analysis. Soil Biol Biochem. 2017;109:35–49.
5. Hu X, Gu H, Liu J, Wei D, Zhu P, Zhou B, Chen X, Jin J, Liu X, Wang G. Metagenomics reveals divergent functional profiles of soil carbon and nitrogen cycling under long-term addition of chemical and organic fertilizers in the black soil region. Geoderma. 2022;418:115846.
6. Pan B, Xia L, Lam SK, Wang E, Zhang Y, Mosier A, et al. A global synthesis of soil denitrification: driving factors and mitigation strategies. Agric Ecosyst Environ. 2022;327:107850.
7. Paustian K, Lehmann J, Ogle S, Reay D, Robertson GP, Smith P. Climate-smart soils. Nature. 2016;532(7597):49–57.
8. Hussain M, Farooq M, Nawaz A, Al-Sadi AM, Solaiman ZM, Alghamdi SS, Ammara U, Ok YS, Siddique KH. Biochar for crop production: potential benefits and risks. J Soils Sediments. 2017;17:685–716.
9. Sharma P, Melkania U. Biochar-enhanced hydrogen production from organic fraction of municipal solid waste using co-culture of *Enterobacter aerogenes* and *E. coli*. Int J Hydrogen Energe. 2017;42(30):18865–74.
10. Tan Z, Lin C, Ji X, Rainey TJ. Returning biochar to fields: a review. Appl Soil Ecol. 2017;116:1–11.
11. Jiang Z, Lian F, Wang Z, Xing B. The role of biochars in sustainable crop production and soil resiliency. J Exp Bot. 2020;71(2):520–42.
12. Liu B, Cai Z, Zhang Y, Liu G, Luo X, Zheng H. Comparison of efficacies of peanut shell biochar and biochar-based compost on two leafy vegetable productivity in an infertile land. Chemosphere. 2019;224:151–61.
13. Yousaf B, Liu G, Wang R, Abbas Q, Imtiaz M, Liu R. Investigating the biochar effects on C-mineralization and sequestration of carbon in soil compared with conventional amendments using the stable isotope ($\delta^{13}C$) approach. GCB Bioenergy. 2017;9(6):1085–99.
14. Ding F, Van Zwieten L, Zhang W, Weng Z, Shi S, Wang J, et al. A meta-analysis and critical evaluation of influencing factors on soil carbon priming following biochar amendment. J Soils Sediments. 2018;18:1507–17.
15. Wang L, Gao C, Yang K, Sheng Y, Xu J, Zhao Y, et al. Effects of biochar aging in the soil on its mechanical property and performance for soil CO_2 and N_2O emissions. Sci Total Environ. 2021;782:146824.
16. Kuppusamy S, Thavamani P, Megharaj M, Venkateswarlu K, Naidu R. Agronomic and remedial benefits and risks of applying biochar to soil: current knowledge and future research directions. Environ Int. 2016;87:1–12.
17. Han M, Zhao Q, Li W, Ciais P, Wang YP, Goll DS, et al. Global soil organic carbon changes and economic revenues with biochar application. GCB Bioenergy. 2022;14(3):364–77.
18. Singh BP, Cowie AL. Long-term influence of biochar on native organic carbon mineralisation in a low-carbon clayey soil. Sci Rep. 2014;4(1):3687.
19. Yu Z, Ling L, Singh BP, Luo Y, Xu J. Gain in carbon: deciphering the abiotic and biotic mechanisms of biochar-induced negative priming effects in contrasting soils. Sci Total Environ. 2020;746:141057.
20. Nguyen BT, Koide RT, Dell C, Drohan P, Skinner H, Adler PR, et al. Turnover of soil carbon following addition of switchgrass-derived biochar to four soils. Soil Sci Soc Am J. 2014;78(2):531–7.
21. Zimmerman AR, Gao B, Ahn MY. Positive and negative carbon mineralization priming effects among a variety of biochar-amended soils. Soil Biol Biochem. 2011;43(6):1169–79.
22. Deciucies S, Whitman T, Woolf D, Enders A, Lehmann J. Priming mechanisms with additions of pyrogenic organic matter to soil. Geochim Cosmochim Acta. 2018;238:329–42.
23. Chen G, Fang Y, Van Zwieten L, Xuan Y, Tavakkoli E, Wang X, et al. Priming, stabilization and temperature sensitivity of native SOC is controlled by microbial responses and physicochemical properties of biochar. Soil Biol Biochem. 2021;154:108139.
24. Mishra U, Hugelius G, Shelef E, Yang Y, Strauss J, Lupachev A, et al. Spatial heterogeneity and environmental predictors of permafrost region soil organic carbon stocks. Sci Adv. 2021;7(9):eaaz5236.
25. Hu T, Zhao B, Li F, Dou X, Hu H, Sun L. Effects of fire on soil respiration and its components in a Dahurian larch (*Larix gmelinii*) forest in Northeast China: implications for forest ecosystem carbon cycling. Geoderma. 2021;402:115273.
26. Wu M, Han X, Zhong T, Yuan M, Wu W. Soil organic carbon content affects the stability of biochar in paddy soil. Agr Ecosyst Environ. 2016;223:59–66.
27. Fang Y, Singh B, Singh BP. Effect of temperature on biochar priming effects and its stability in soils. Soil Biol Biochem. 2015;80:136–45.
28. Sheng Y, Zhu L. Biochar alters microbial community and carbon sequestration potential across different soil pH. Sci Total Environ. 2018;622:1391–9.
29. Wang J, Xiong Z, Kuzyakov Y. Biochar stability in soil: meta-analysis of decomposition and priming effects. GCB Bioenergy. 2016;8(3):512–23.
30. Sui X, Wang L, Lv X, Liu Y, Zhu Y, Fan L, Wang H. Influence of composite amendments on the characteristics of sandy soil. Sustainability. 2025;17:7619. https://doi.org/10.3390/su17177619.
31. Luo Y, Durenkamp M, De Nobili M, Lin Q, Brookes P. Short term soil priming effects and the mineralisation of biochar following its incorporation to soils of different pH. Soil Biol Biochem. 2011;43(11):2304–14.
32. Yang C, Xing F, Zhu J, Li R, Zhang Z. Temporal and spatial distribution, utilization status, and carbon emission reduction potential of straw resources in China. Chin J Environ Sci. 2023;44(2):1149–62.
33. Xia L, Cao L, Yang Y, Ti C, Liu Y, Smith P, et al. Integrated biochar solutions can achieve carbon-neutral staple crop production. Nat Food. 2023;4(3):236–46.
34. Lu B, Song L, Zang S, Wang H. Warming promotes soil CO_2 and CH_4 emissions but decreasing moisture inhibits CH_4 emissions in the permafrost peatland of the great xing'an mountains. Sci Total Environ. 2022;829:154725.
35. Song L, Zang S, Lin L, Lu B, Sun C, Jiao Y, Wang H. Responses of nitrous oxide fluxes to autumn freeze–thaw cycles in permafrost peatlands of the Da xing'an Mountains, Northeast China. Environ Sci Pollut Res. 2022;29:31700–12.
36. Kerré B, Hernandez-Soriano MC, Smolders E. Partitioning of carbon sources among functional pools to investigate short-term priming effects of biochar in soil: a ^{13}C study. Sci Total Environ. 2016;547:30–8.
37. Cross A, Sohi SP. The priming potential of biochar products in relation to labile carbon contents and soil organic matter status. Soil Biol Biochem. 2011;43(10):2127–34.
38. Wang H, Wang X, Teng H, Xu J, Sheng L. Purification mechanism of city tail water by constructed wetland substrate with NaOH-modified corn straw biochar. Ecotoxicol Environ Saf. 2022;238:113597.
39. Liu R, Zang S, Zhao L, Wu X, Liu L, Wu S, et al. Climate and environmental changes in the Mohe basin permafrost region of the Greater Hinggan Mountains since 30 ka BP. Acta Geogr Sin. 2024;79(9):2280–96.
40. Liu X, Wang Q, Qi Z, Han J, Li L. Response of N_2O emissions to biochar amendment in a cultivated sandy loam soil during freeze-thaw cycles. Sci Rep. 2016;6:35411.
41. Hawthorne I, Johnson M, Jassal R, Black T, Grant N, Smukler S. Application of biochar and nitrogen influences fluxes of CO_2, CH_4 and N_2O in a forest soil. J Environ Manage. 2017;192:203–14.
42. Chen L, Liang J, Qin S, Liu L, Fang K, Xu Y, Ding J, Li F, Luo Y, Yang Y. Determinants of carbon release from the active layer and permafrost deposits on the Tibetan plateau. Nat Commun. 2016;7(1):13046.
43. Lang M, Cai Z, Chang SX. Effects of land use type and incubation temperature on greenhouse gas emissions from Chinese and Canadian soils. J Soils Sediments. 2011;11:15–24.
44. Cai Y, Wang X, Ding W, Tian L, Zhao H, Lu X. Potential short-term effects of Yak and Tibetan sheep dung on greenhouse gas emissions in two alpine grassland soils under laboratory conditions. Biol Fertil Soils. 2013;49:1215–26.
45. Shaikh SM, Nasser MS, Hussein I, Benamor A, Onaizi SA, Qiblawey H. Influence of polyelectrolytes and other polymer complexes on the flocculation and rheological behaviors of clay minerals: a comprehensive review. Sep Purif Technol. 2017;187:137–61.
46. Burrell LD, Zehetner F, Rampazzo N, Wimmer B, Soja G. Long-term effects of biochar on soil physical properties. Geoderma. 2016;282:96–102.
47. Liang B, Lehmann J, Sohi SP, Thies JE, O'neill B, Trujillo L, Gaunt J, Solomon D, Grossman J, Neves EG. Black carbon affects the cycling of non-black carbon in soil. Org Geochem. 2010;41(2):206–13.
48. Wang H, Teng H, Wang X, Xu J, Sheng L. Physicochemical modification of corn straw biochar to improve performance and its application of constructed wetland substrate to treat city tail water. J Environ Manage. 2022;310:114758.
49. Gao S, Deluca TH, Cleveland CC. Biochar additions alter phosphorus and nitrogen availability in agricultural ecosystems: a meta-analysis. Sci Total Environ. 2019;654:463–72.
50. Karimi A, Moezzi A, Chorom M, Enayatizamir N. Application of biochar changed the status of nutrients and biological activity in a calcareous soil. J Soil Sci Plant Nutr. 2020;20:450–9.
51. Zhang H, Voroney R, Price G. Effects of temperature and processing conditions on biochar chemical properties and their influence on soil C and N transformations. Soil Biol Biochem. 2015;83:19–28.

52. Dong X, Guan T, Li G, Lin Q, Zhao X. Long-term effects of biochar amount on the content and composition of organic matter in soil aggregates under field conditions. J Soils Sediments. 2016;16:1481–97.
53. Zhu K, Li W, Yang S, Ran Y, Lei X, Ma M, Wu S, Huang P. Intense wet-dry cycles weakened the carbon sequestration of soil aggregates in the riparian zone. CATENA. 2022;212:106117.
54. Mustafa A, Xu M, Shah SA, Abrar MM, Sun N, Wang B, Cai Z, Saeed Q, Naveed M, Mehmood K. Soil aggregation and soil aggregate stability regulate organic carbon and nitrogen storage in a red soil of Southern China. J Environ Manag. 2020;270:110894.
55. Smebye A, Alling V, Vogt RD, Gadmar TC, Mulder J, Cornelissen G, Hale SE. Biochar amendment to soil changes dissolved organic matter content and composition. Chemosphere. 2016;142:100–5.
56. Guo K, Zhao Y, Liu Y, Chen J, Wu Q, Ruan Y, et al. Pyrolysis temperature of biochar affects ecoenzymatic stoichiometry and microbial nutrient-use efficiency in a bamboo forest soil. Geoderma. 2020;363:114162.
57. Chen X, Chen G, Chen L, Chen Y, Lehmann J, Mcbride MB, Hay AG. Adsorption of copper and zinc by biochars produced from pyrolysis of hardwood and corn straw in aqueous solution. Bioresour Technol. 2011;102(19):8877–84.
58. Dong X, Singh BP, Li G, Lin Q, Zhao X. Biochar has little effect on soil dissolved organic carbon pool 5 years after biochar application under field condition. Soil Use Manage. 2019;35(3):466–77.
59. Lei Z, Li Q, Song X, Wang W, Zhang Z, Peng C, et al. Biochar mitigates dissolved organic carbon loss but does not affect dissolved organic nitrogen leaching loss caused by nitrogen deposition in Moso bamboo plantations. Glob Ecol Conserv. 2018;16:e00494.
60. Ren T, Liao J, Delgado-Baquerizo M, Ni J, Li Y, Jin L, Ruan H. Organic fertilization promotes the accumulation of soil particulate organic carbon in a 9-year plantation experiment. Land Degrad Dev. 2023;34(15):4741–50.
61. Li Y, Hu S, Chen J, Müller K, Li Y, Fu W, et al. Effects of biochar application in forest ecosystems on soil properties and greenhouse gas emissions: a review. J Soils Sediments. 2018;18(2):546–63.
62. Luo Z, Baldock J, Wang E. Modelling the dynamic physical protection of soil organic carbon: insights into carbon predictions and explanation of the priming effect. Glob Change Biol. 2017;23(12):5273–83.
63. Long X, Yu Z, Liu S, Gao T, Qiu R. A systematic review of Biochar aging and the potential eco-environmental risk in heavy metal contaminated soil. J Hazard Mater. 2024;472:134345.
64. Hagemann N, Joseph S, Schmidt HP, Kammann CI, Harter J, Borch T, et al. Organic coating on biochar explains its nutrient retention and stimulation of soil fertility. Nat Commun. 2017;8(1):1089.
65. Archanjo BS, Mendoza ME, Albu M, Mitchell DRG, Hagemann N, Mayrhofer C, et al. Nanoscale analyses of the surface structure and composition of biochars extracted from field trials or after co-composting using advanced analytical electron microscopy. Geoderma. 2017;294:70–9.
66. Rasul M, Cho J, Shin HS, Hur J. Biochar-induced priming effects in soil via modifying the status of soil organic matter and microflora: a review. Sci Total Environ. 2022;805:150304.
67. Walpen N, Lau MP, Fiskal A, Getzinger GJ, Meyer SA, Nelson TF, Lever MA, Schroth MH, Sander M. Oxidation of reduced peat particulate organic matter by dissolved oxygen: quantification of apparent rate constants in the field. Environ Sci Technol. 2018;52(19):11151–60.
68. Nie T, Yang X, Chen H, Müller K, Shaheen SM, Rinklebe J, et al. Effect of biochar aging and co-existence of diethyl phthalate on the mono-sorption of cadmium and zinc to biochar-treated soils. J Hazard Mater. 2021;408:124850.
69. Ren X, Wang F, Zhang P, Guo J, Sun H. Aging effect of minerals on biochar properties and sorption capacities for atrazine and phenanthrene. Chemosphere. 2018;206:51–8.
70. Walkiewicz A, Kalinichenko K, Kubaczyński A, Brzezińska M, Bieganowski A. Usage of biochar for mitigation of CO_2 emission and enhancement of CH_4 consumption in forest and orchard haplic luvisol (Siltic) soils. Appl Soil Ecol. 2020;156:103711.
71. Deng X, Teng F, Chen M, Du Z, Wang B, Li R, Wang P. Exploring negative emission potential of Biochar to achieve carbon neutrality goal in China. Nat Commun. 2024;15(1):1085.
72. Yang Y, Sun K, Han L, Chen Y, Liu J, Xing B. Biochar stability and impact on soil organic carbon mineralization depend on biochar processing, aging and soil clay content. Soil Biol Biochem. 2022;169:108657.
73. Nguyen TTN, Xu C, Tahmasbian I, Che R, Xu Z, Zhou X, et al. Effects of biochar on soil available inorganic nitrogen: a review and meta-analysis. Geoderma. 2017;288:79–96.
74. Sapkota S, Ghimire R, Bista P, Hartmann D, Rahman T, Adhikari S. Greenhouse gas mitigation and soil carbon stabilization potential of forest biochar varied with biochar type and characteristics. Sci Total Environ. 2024;931:172942.
75. Pei J, Li J, Mia S, Singh B, Wu J, Dijkstra FA. Biochar aging increased microbial carbon use efficiency but decreased biomass turnover time. Geoderma. 2021;382:114710.
76. Wiesenberg GL, Schwarzbauer J, Schmidt MW, Schwark L. Plant and soil lipid modification under elevated atmospheric CO_2 conditions: part II. Stable carbon isotopic values ($\delta^{13}C$) and turnover. Org Geochem. 2008;39(1):103–17.
77. Bowling DR, Pataki DE, Randerson JT. Carbon isotopes in terrestrial ecosystem pools and CO_2 fluxes. New Phytol. 2008;178(1):24–40.
78. Kuzyakov Y, Review. Factors affecting rhizosphere priming effects. J Plant Nutr Soil Sci. 2010;165(4):66–70.
79. Kuzyakov Y, Bol R. Sources and mechanisms of priming effect induced in two grassland soils amended with slurry and sugar. Soil Biol Biochem. 2006;38(4):747–58.
80. Joseph SD, Camps-Arbestain M, Lin Y, Munroe P, Chia C, Hook J, et al. An investigation into the reactions of Biochar in soil. Soil Res. 2010;48(7):501–15.
81. Mitra D, Mondal R, Khoshru B, Senapati A, Radha T, Mahakur B, Uniyal N, Myo EM, Boutaj H. Sierra B E G. Actinobacteria-enhanced plant growth, nutrient acquisition, and crop protection: advances in soil, plant, and microbial multifactorial interactions. Pedosphere. 2022;32(1):149–70.
82. Fan K, Weisenhorn P, Gilbert JA, Shi Y, Bai Y, Chu H. Soil pH correlates with the co-occurrence and assemblage process of diazotrophic communities in rhizosphere and bulk soils of wheat fields. Soil Biol Biochem. 2018;121:185–92.
83. Fu Y, Luo Y, Auwal M, Singh BP, Van Zwieten L, Xu J. Biochar accelerates soil organic carbon mineralization via rhizodeposit-activated actinobacteria. Biol Fertil Soils. 2022;58(5):565–77.
84. Zhang F, Hou Y, Zed R, Mauchline TH, Shen J, Zhang F, et al. Root exudation of organic acid anions and recruitment of beneficial actinobacteria facilitate phosphorus uptake by maize in compacted silt loam soil. Soil Biol Biochem. 2023;184:109074.
85. Spokas K, Koskinen W, Baker J, Reicosky D. Impacts of woodchip biochar additions on greenhouse gas production and sorption/degradation of two herbicides in a Minnesota soil. Chemosphere. 2009;77(4):574–81.
86. Le Mer J, Roger P. Production, oxidation, emission and consumption of methane by soils: a review. Eur J Soil Biol. 2001;37(1):25–50.
87. Kotiaho M, Fritze H, Merilä P, Juottonen H, Leppälä M, Laine J, et al. Methanogen activity in relation to water table level in two boreal fens. Biol Fertil Soils. 2010;46:567–75.
88. Liu Y, Yang M, Wu Y, Wang H, Chen Y, Wu W. Reducing CH_4 and CO_2 emissions from waterlogged paddy soil with biochar. J Soils Sediments. 2011;11:930–9.
89. Wang H, Guo C, Wang S, Chu X, Zhang J, Wang C, et al. Insights into the thermal insulation capability of a new polyurethane polymer subgrade material: an in-situ field test on the Qinghai-Tibet highway. Transp Geotech. 2024;46:101240.

Publisher's note